IEEE Access
Multidisciplinary | Rapid Review | Open Access Journal

Received June 12, 2021, accepted June 22, 2021, date of publication June 28, 2021, date of current version July 16, 2021.

Digital Object Identifier 10.1109/ACCESS.2021.3092997

Design, Analysis, and Optimization of the Array of Axial Rectangular Slots on a Cylindrical Waveguide

MAHMOUD SHARAFI MASOULEH, AMIN KARGAR BEHBAHANI, AND MALEK ADJOUADI

Center for Advanced Technology and Education, Department of Electrical and Computer Engineering, Florida International University, Miami, FL 33174, USA

Corresponding author: Mahmoud Sharafi Masouleh (mshar052@fiu.edu)

This work was supported by the National Science Foundation (NSF) under Grant CNS-1920182, Grant CNS-1532061, Grant CNS-1338922, Grant CNS-2018611, and Grant CNS-1551221.

ABSTRACT In the current work, for the first time, the design equations for an array of rectangular slots axially placed on a cylindrical waveguide are driven and presented, making it possible to attain asymmetrical and non-broadside patterns with higher bandwidths. The method of least squares is then used for both the radiation pattern synthesis with the specified side lobe level and the array input impedance matching. For optimization, the error function comprised of the three terms of impedance matching, array pattern synthesis, and slot design equations is constructed. To minimize the error function, the genetic algorithm combined with the conjugate gradient method is utilized and the geometrical characteristic of the slots defined. This procedure increases the design speed and provides the means to synthesize any desired pattern for an array of axial rectangular slots on a cylindrical waveguide. Numerical and fabrication examples are presented as illustrations of the proposed synthesis method. The results of the proposed method are verified by using the commercial software High-Frequency Structure Simulator (HFSS) in comparison to measurement results obtained out of the proposed prototype of a fabricated antenna operating at the frequency of 9 GHz.

INDEX TERMS Slotted cylindrical antenna, axial slot array, design equations, method of least squares (MLS), genetic algorithms.

I. INTRODUCTION

In the literature, extensive analysis of different antenna topologies with different shapes and designs is reported. They all show distinctive and systematic design procedures that characterize their proposed antennas [1]–[3]. In the designs, optimization techniques are applied to enhance the antenna's parameters and study the effect of different dimensions and materials on parameters [4]. Deployment, manufacturing techniques, and production procedures have all been widely investigated at microwave frequencies for the different application domains, ranging from medical wearable applications to radars [5]–[8].

Many different antenna types are used in radio systems with specialized properties for particular applications [9]–[10].

The associate editor coordinating the review of this manuscript and approving it for publication was Mingchun Tang.

Based on the target application, antenna parameters, including desired frequency, gain, bandwidth, impedance, and polarization, and the shape and the configuration of the antenna should be calculated and designed [11]. Despite confronting the constraints and many limitations in antenna design, novel methods have been proposed to improve the antenna parameters and optimize antenna size [12].

However, the slot array antennas have attracted significant attention due to their inherent valued characteristics of high radiation efficiency, high gain, wide bandwidth, and low losses. Consequently, they may be preferable to reflector and patch antennas [13]. The design of slot arrays goes back to 1948 when Stevenson [14] carried out the preliminary analysis on resonant slot arrays for the first time. This analysis was initially proposed by Oliner in the study on non-resonant slots [15]. However, Elliot was the one who presented the design equations for slot arrays on a rectangular waveguide [16]. In the study by Oraizi *et al.* [17], a design algorithm for an edge slot array is proposed with

This work is licensed under a Creative Commons Attribution 4.0 License. For more information, see https://creativecommons.org/licenses/by/4.0/

non-uniform spacing on a rectangular waveguide. Slotted arrays on a cylindrical waveguide were initially studied by Wait [18]. In [19], Shin and Eom studied the radiation from multiple circumferentially opened rectangular slots displaced along the longitudinal direction. Masouleh and Behbahani in [20] extended Shin's work by proposing a similar method but for circumferential slots placed on a cylindrical waveguide. In this work, the design equations are proposed for rectangular slots elongated along the axis of the cylinder forming a linear array with the intent to broaden bandwidth and hence the realm of practicality. With their high gain, efficiency, mechanical strength, and absence of spurious radiation from their feeding system, slot array antennas have been deployed effectively in numerous applications involving radar and communication systems and continue to many other practical implications [21]–[23]. However, despite all these research endeavors, slot array antenna, axially placed on a cylindrical waveguide, is not well-covered in the literature.

In this study, a method is proposed to design narrow axially rectangular slots on a conducting cylinder. The advantage of this design compared to the circumferentially disposed slot arrays [24] is their wider bandwidth [25]. The method follows the approach introduced by Elliot [26] that devised a recursive procedure for the design of longitudinal slot arrays by considering the external mutual coupling. For the array design and the pattern synthesis, three main variables are considered: length of slots L, slots' center-to-center distance "d," and their disposed angle φ_0. To synthesize the radiation pattern with specified sidelobe level and for the impedance matching of the array input, the method of least squares is applied. The minimization of the error function is performed using a genetic algorithm (GA) and the conjugate gradient (CG) method. Through this work and for the first time, an analytical method is proposed for both purposes, i.e., the design equations and the synthesis of an array composed of rectangular slots arranged along the central axis of a cylindrical waveguide. The results are verified using the HFSS commercial software, and the measurements are obtained via the proposed prototype built for this purpose.

II. FORMULATION

A. FIRST AND SECOND DESIGN EQUATIONS

An array of narrow rectangular waveguide slots on a cylindrical waveguide is shown in Fig.1. Each slot is of length L, while the center-to-center distance between two consecutive slots is d. Two design equations are derived for the array based on the physical characteristics L, d, and arch length (φ_0). From these two equations, the information of both the mutual and self-impedance/admittance of the slots is seen to define the array's characteristics. For the pattern synthesis problem, an error function is also developed. The developed error function comprises three terms: impedance matching, array pattern synthesis, and slot design equations. Its minimization is achieved by the combination of the GA and CG methods.

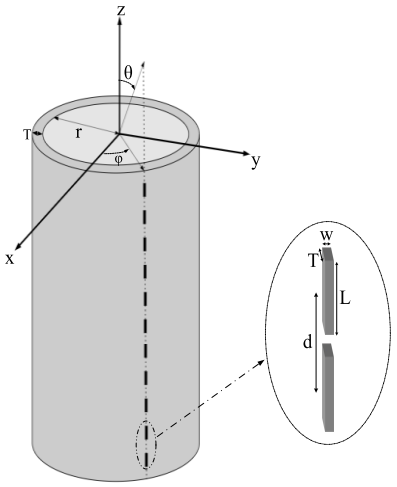

FIGURE 1. An array of narrow rectangular slots along the axis of the cylindrical waveguide.

Due to the orientation of the slots, the circular waveguide is assumed to operate in its dominant mode TE_{11}. Every slot is excited by a tangential electric field on its aperture as follows:

$$E_\varphi = E_{\tan} = \frac{V_n^s}{w_n}\cos\left(\frac{\pi z}{L_n}\right), \quad \frac{L_n}{2} < z < \frac{L_n}{2} \tag{1}$$

With

$$E_s = E_\varphi \bar{u}_\varphi \quad E_Z = 0 \tag{2}$$

where W_n and L_n are the width and length of the n 'th slot, respectively, with V_n^s being the maximum voltage distributed across the n 'th slot.

Following the procedure that is presented in appendix A, the two design equations are defined as follows:

First Design equation:

$$\frac{Z_n^a}{Z_0} = \mathrm{Kf}_n \frac{V_n^s}{I_n} \tag{3}$$

Second Design equation:

$$\frac{Z_n^a}{Z_0} = \frac{\eta^2}{2} Z_0 |K|^2 \frac{f_n^2}{Z_n^{d,a}} \tag{4}$$

where:

$$\mathrm{f}_n = \frac{L_n cos\left(\frac{\beta_{11}L_n}{2}\right) cos\left(\varphi_{0\mathrm{n}}\right)}{\left(\pi^2 - (\beta_{11}L_n)^2\right)} \tag{5}$$

and

$$K = -j\sqrt{\frac{4\pi h^2 J_1^2(ha)}{\omega\mu\beta_{11}Z_0\left[\int_0^a\left(\frac{J_1^2(h\rho)}{h^2\rho} + \rho J_1'^2(h\rho)\right)d\rho\right]}} \tag{6}$$

In these equations, I_n, V_n^s and Z_n^a are the mode current, the slot's voltage, and the active impedance of the n'th slot, respectively. As is the active loaded dipole impedance, defined as follows:

$$Z_n^{d,a} = Z_{nn} + Z_n^b \tag{7}$$

where Z_{nn} is the axial slot-impedance and Z_n^b is the mutual impedance between the two axial slots. The complete derivations of Z_{nn} and Z_n^b are presented in Appendix B.

It should be noted that based on the two design equations, the length of the slots and their azimuthal locations can be determined. These equations work in the microwave range of frequency, but we need to take the skin effect and the waveguide power loss consideration into account for the upper bands.

The next step is to define the error function. This will be done based on an equivalent circuit model for the proposed array.

III. THE ERROR FUNCTION

The error function is comprised of the three terms of impedance matching, slot design equations, and pattern synthesis. For each term, a single error function is constructed. All of the error functions are summed up at the end into one to produce the final error function.

A. ACTIVE IMPEDANCE MATCHING ERROR FUNCTION

For the active impedance matching, the method of least squares is used where both the real and imaginary parts are minimized.

$$\varepsilon_{Matching} = W_1 \left| \mathrm{Re}\left(\frac{Y_n}{G_0}\right) - 1 \right|^2 + W_2 \left| \mathrm{Im}\left(\frac{Y_n}{G_0}\right) \right|^2 \quad (8)$$

where W_1 and $W2$ are weigh functions of error function.

For linear array longitudinal slots in a cylindrical waveguide, the equivalent circuit model with a matched load in its end is shown in Fig. 2.

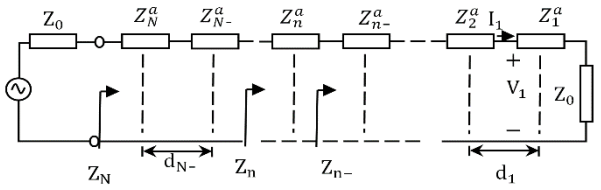

FIGURE 2. The equivalent circuit of axial slot array.

In Fig. 2, the equivalent circuit of the linear traveling wave axial slot array, modeled by a transmission line with a series impedance, is shown. As seen, I_i is the constant parameter across the slots, so the slot's voltage distribution which is proportional to the cosine form of voltage, just depends on the length of the slot.

B. SLOT DESIGN EQUATION ERROR FUNCTION

According to the design procedure described in [26], the normalized admittance of the n'th slot is:

$$\frac{Z_n}{Z_0} = \frac{K_1 f_n^2}{Z_n^a} + \frac{(Z_{n-1}/Z_0)\cos\beta_{11}d_{n-1} + j\sin\beta_{11}d_{n-1}}{\cos\beta_{11}d_{n-1} + j\,(Z_{n-1}/Z_0)\sin\beta_{11}d_{n-1}} \quad (9)$$

Since the current of two successive elements can be written as:

$$\begin{aligned} I_n &= I_{n-1}\cos\beta_{11}d_{n-1} + jI_{n-1}Y_0\sin\beta_{11}d_{n-1} \\ &= I_{n-1}\left[\cos\beta_{11}d_{n-1} + j\left(\frac{Z_{n-1}}{Z_0}\right)\sin\beta_{11}d_{n-1}\right] \end{aligned} \quad (10)$$

Considering equations (9) and (10), the following relationship can be established:

$$\begin{aligned} &\cos(\beta_{11}d_{n-1}) + j\frac{Z_{n-1}}{Z}\sin(\beta_{11}d_{n-1}) \\ &\qquad = \frac{V_n^s}{V_{n-1}^s}\cdot\frac{f_n}{f_{n-1}}\cdot\frac{Z_{n-1}^a/Z_0}{Z_n^a/Z_0} \end{aligned} \quad (11)$$

Furthermore, the error function can be written as:

$$\begin{aligned} \varepsilon_{DesignEqs.} = w_3 \Bigg| &\sum_{n=2}^{N} \cos\beta d_{n-1} + j\frac{Z_{n-1}}{Z_0}\sin\beta d_{n-1} \\ &- \frac{V_n^s}{V_{n-1}^s}\cdot\frac{f(\varphi_n, L_n)}{f(\varphi_{n-1}, L_{n-1})}\cdot\frac{Z_{n-1}^a/Z_0}{Z_{n-1}^a/Z_0}\Bigg|^2 \end{aligned} \quad (12)$$

C. PATTERN SYNTHESIS ERROR FUNCTION

1) A RELATION FOR THE RADIATION PATTERN OF AXIAL SLOT ARRAY

The radiation pattern of an array of axial slots on a cylinder as defined in [6] are replicated here in conformance with the proposed design approach:

$$E_\theta(r\to\infty) = j\omega\mu\frac{e^{-jkr}}{\pi r}\sin(\theta)\sum_{m=-\infty}^{\infty} e^{jm\phi}j^{m+1}f_m(\omega) \quad (13)$$

$$E_\phi(r\to\infty) = -jk\frac{e^{-jkr}}{\pi r}\sin(\theta)\sum_{m=-\infty}^{\infty} e^{jm\phi}j^{m+1}g_m(\omega) \quad (14)$$

The Fourier transforms $f_m(\omega)$ and $g_m(\omega)$ can be obtained by using equations (1) and (2) and also invoking the appropriate boundary conditions:

$$f_m(\omega) = 0 \quad (15)$$

$$g_m(\omega) = \frac{\bar{E}_\varphi(m,w)}{\sqrt{(k^2-w^2)}H_m^{(2)'}\left(R\sqrt{k^2-w^2}\right)} \quad (16)$$

$$\bar{E}_\varphi(m,w) = \sum_{p=1}^{P}\sum_{n=1}^{N}\frac{V_{pn}L_{pn}\cos\left(\frac{wL_{pn}}{2}\right)}{a\left(\pi^2-\left(wL_{pn}\right)^2\right)}e^{-j(m\varphi_{pn}+wz_{pn})} \quad (17)$$

where P denotes the number of columns of the axial slot. The far-field components consist of E_θ and $\bar{E}_\varphi$. Therefore, the E-plane pattern is considered only with the E_θ field component.

For the appearance of some null-points in the pattern, we considered the asymmetrical modified Taylor pattern as in [16]:

$$h_k = \frac{\sin(\pi u)}{\pi u}\frac{\prod_{n=-(\hat{n}_L-1)}^{\hat{n}_R-1}\left(1-u/\hat{u}_n\right)}{\prod_{n=-(\hat{n}_L-1)}^{\hat{n}_R-1}(1-u/n)} \quad (18)$$

where h_k is the asymmetrical modified Taylor pattern, and also R and L denote the right and left components of the Taylor pattern, respectively. The unit normal factors for both the right and left part are as defined below:

$$\hat{u}_n = \hat{n}_R \left[\frac{A_R^2 + \left(n - \frac{1}{2}\right)^2}{A_R^2 + \left(\hat{n} - \frac{1}{2}\right)^2} \right]^{1/2} \qquad n = 1, 2, \ldots, \hat{n}_R - 1 \quad (19)$$

and

$$\hat{u}_n = -\hat{n}_L \left[\frac{A_L^2 + \left(n + \frac{1}{2}\right)^2}{A_L^2 + \left(\hat{n} - \frac{1}{2}\right)^2} \right]^{1/2} \times n = -\left(\hat{n}_L - 1\right), \ldots, -2, -1 \quad (20)$$

where $R = 10^{(SLL/20)}, A = \frac{1}{n}\cosh^{-1}(R)$, and with A_L and A_R defining the left and right side lobe level (SLL), respectively. For A_L and A_R, we use the left SLL and right SLL, respectively. The pattern's main lobe elevation angle depends only on the spacing of the slots. This condition happens only when higher-order grating lobes appear in the pattern. Otherwise, the change of the elevation angle is about 1 to 3 degrees.

Having defined the radiation pattern function using the method of least squares, the error function can be defined as:

$$\varepsilon_{\text{Synyhesis}} = \sum_{k=1}^{K} w_k \left(|F(\theta_k) - h_k|\right)^2 \quad (21)$$

where

$$F = 20\log\left(\left|\frac{E_\theta}{E_{\theta\max}}\right|\right) \quad (22)$$

It is worth mentioning that the error function depends on the spacing between the slots and the slots' dimensions. The error function in total is the combination of the errors determined through equations (8), (12), and (21) as follows:

$$\varepsilon_{Error\ Function} = \varepsilon_{\text{Matching}} + \varepsilon_{\text{DesignEquations.}} + \varepsilon_{\text{Synyhesis}} \quad (23)$$

Through the optimization process, the following sections show how the most desired pattern can be obtained.

IV. SYNTHESIS OF AN AXIAL SLOT ARRAY ON THE CYLINDRICAL WAVEGUIDE WITH A MODIFIED TAYLOR PATTERN AT 9 GHz

To determine the error function, both the space between adjacent slots and the length of the slots are assumed identical. These assumptions will result in the simplicity of the calculation process to minimize computational time. On the other hand, the equality of length of slots makes the amplitude of voltage distributions in the slots even and equal.

A cylindrical array with twenty-two axial slots consisting of two rows of 11 elements is designed, as shown in Fig 3. The length of the slot and the spacing between slots were optimized, the minimization of the error function is performed by combining a genetic algorithm (GA) with the conjugate gradient (CG) method, and the parameters are as given in Table 1. The spacing between adjacent slots is equal to 19.88 mm. The width and length of the slots are equal to 3 mm and 10.95 mm, respectively. Hence, optimization of these parameters aims to yield better impedance matching and the desired pattern shape.

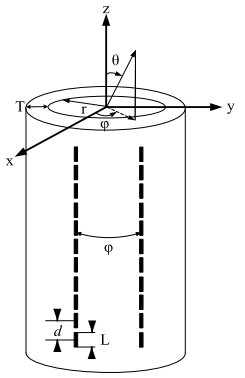

FIGURE 3. Two-column narrow rectangular slot array on a cylindrical waveguide.

TABLE 1. Characteristics of structure optimized parameters and desired pattern antenna, for example.

Antenna parameters	N: Number of slots	Two by eleven
	W: Slot width	3.00 mm
	T: Thickness of wall of the waveguide	2.80 mm
	R: Radius of waveguide cylinder	11.26 mm
	Operation frequency	9.00 GHz

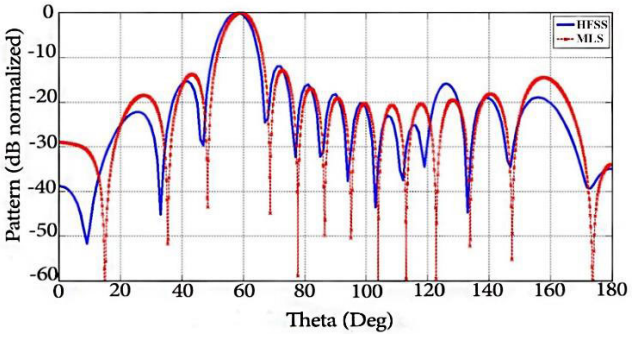

FIGURE 4. E-plane pattern cut comparison between MLS and HFSS at 9GHz in XZ-plane for $\varphi = 0$.

For comparative purposes, the pattern of the slot array as obtained by the method of least squares (MLS) and HFSS software simulation (at 9 GHz in XZ-plane for $\varphi = 0$) as shown in Fig. 4. As shown in Fig. 4, more specifically about the main beam, the MLS design pattern matches well with the HFSS simulation pattern, and the sidelobe levels are almost between the specified design constraints. The inability to

reach the specified sidelobe levels is mainly due to internal mutual coupling, which is a factor that was not counted in the design. The assumption of sinusoidal field distribution in the slot is another possible source of error. The VSWR of the array simulated by HFSS at the input terminal of the cylindrical waveguide is shown in Fig. 5, reflecting that the high bandwidth of the designed antenna is about 200 MHz.

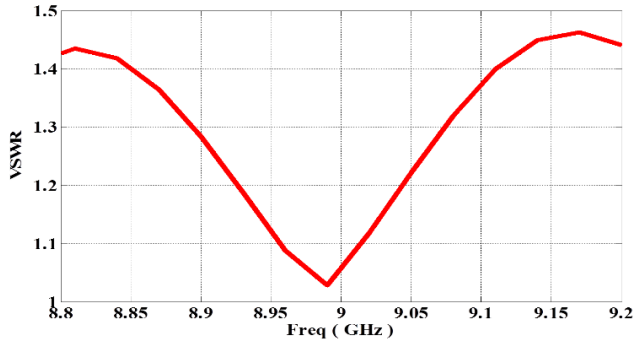

FIGURE 5. Simulated results of VSWR.

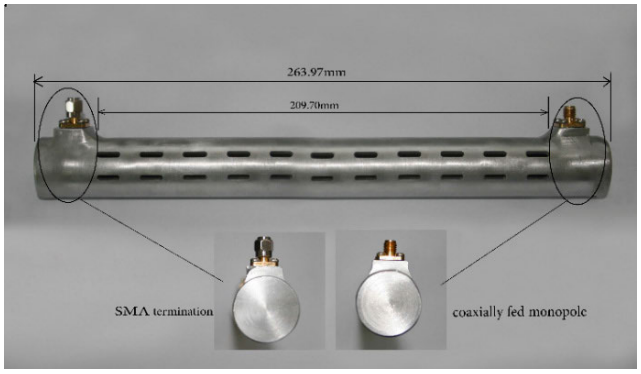

FIGURE 6. Fabrication of the 22-slot antenna (two rows of 11 elements). All slots are identical, and the distance between two adjacent slots is d = 19.88 mm.

V. FABRICATION, MEASUREMENT, AND COMPARISON

As shown in Fig. 6, a typical axial slot array antenna consisting of two rows of 11 slots on a cylindrical waveguide is fabricated for the test, and measurement results are provided to clarify the accuracy of the acquired design equations. The fabricated antenna consists of a coaxially fed monopole, a slotted cylinder, and an SMA termination. The antenna has two ports, and a 50-Ohm male pin SMA as a terminator coax connector plug (TCCP) is used to absorb the reflected waves on one side, while the other port is to serve as the excitatory terminal of the antenna. The coaxially fed monopole, which has a protruding inner conductor of 6.9882 mm length, excites the TE_{11} mode into the slotted circular cylinder. The SMA termination used in the measurements demonstrates SWR below 1.25 at 9 GHz [28].

Fig. 7 illustrates the simulated and measured return losses of the fabricated slot array antenna. The measured return loss is less than −17 dB from 8.9 GHz to 9.1 GHz. The difference between the simulation and measurement results, as seen

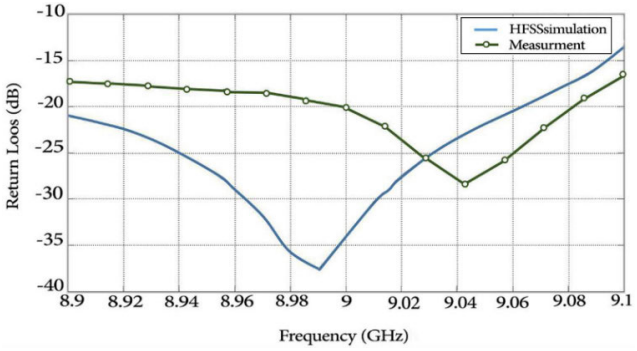

FIGURE 7. Measured and simulated return loss (S_{11}) versus frequency.

TABLE 2. Characteristics of structure optimized parameters and desired pattern antenna.

Antenna parameters	N: Number of slots	Two by eleven
	W: Slot width	3.00 mm
	T: Thickness of wall of the waveguide	2.80 mm
	R: Radius of waveguide cylinder	11.26 mm
	Operation frequency	9.00 GHz
Optimized parameters	L: Slot length	10.95 mm
	d: Space of slots	19.88 mm
	$\varphi_{1\&2}$: Slot offset	-13.55^0 & 27.43^0
Characteristics of the desired pattern	Modified Taylor pattern to have SLL_L= -15 dB SLL_R= -12 dB	

in Fig. 7, can be attributed to milling machine fabrication process tolerance. Our theoretical model could not mimic the reflection, which is possibly introduced by the coaxially fed monopole and the SMA termination.

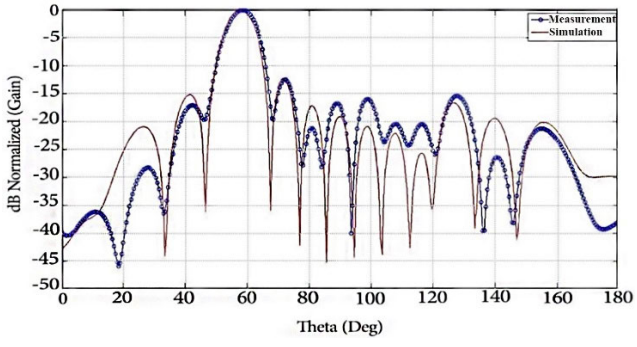

FIGURE 8. Measured and simulated radiation patterns for an axial slot at operating frequency f = 9 GHz.

The antenna radiation pattern is measured and compared to the simulation pattern at 9 GHz, as shown in Fig. 8. The results obtained for the prototyped antenna have good compliance with the design goal, that SLL is lower than −15dB in the H-Plane.

As the graphs in Figures 4, 7, and 8 reveal, there are strong agreements in the overall behavior of the measured and simulated outcomes, which verify the accuracy of the proposed method. The proposed antenna structure, which is designed based on acquired equations, can be used as a phased array antenna to scan a range of space. This feature comes out of the antenna's high bandwidth, which by changing the frequency from one to another in a specific range, the angle of the main lobe gets changed consequently, and it can sweep a range of space to find targets. It is worth mentioning that since the amplitude of the voltage distribution is even across the waveguide, it is possible to change the beam angle but just by frequency changing. Moreover, for designing wideband omnidirectional slotted-waveguide antenna arrays, more columns of slots can be placed around the waveguide. However, it should be noticed that because ripples amplitude is proportional to the number of slots distributed around the circumference of the waveguide, increasing the number of slots just for the sake of having an omnidirectional pattern increases the level of ripple in the omnidirectional radiation pattern (azimuthal plane).

VI. CONCLUSION

The proposed study expanded on the method of least squares for the synthesis of axial slot array on a cylindrical waveguide for the dominant mode TE_{11} and analyzed the radiation from axial slots on a cylindrical waveguide. Using Elliott's method [16] as a baseline, and for the first time, the design equations were presented and expanded for the traveling wave mode with the use of equivalent circuits for axial slot array antenna. Subsequently, the geometrical dimensions of the slot array on the cylindrical surface were determined by minimizing the appropriate error functions. This minimization led to accurate pattern synthesis impedance matching, formulation of the relevant design equations, and minimization of power losses. With the proposed antenna design, the computational requirements were optimized. The method is also advantageous because it combines the determination of slots' parameters and impedance matching with the array pattern synthesis, leading to a quick design with higher accuracy.

Moreover, a design example was presented to demonstrate the effectiveness of the proposed synthesis method on a cylindrical slot array. Full-wave simulation software HFSS was used to verify the proposed design procedure. To verify the accuracy and the practical feasibility of the simulation, measurements were taken on a prototype design of an array of axial slots on a cylindrical waveguide, and good correspondence with the theoretical predictions was achieved.

NOMENCLATURE

L	length of slots
d	slots' center-to-center distance
φ_0	disposed angle
W_n	width of the n'th slot
L_n	length of n'th slot
V_n^s	voltage distributed across the slot
I_n	mode current
V_n^s	Slot's voltage
Z_n^a	the active impedance of the nth slot
Z_{nn}	the axial slot-impedance
Z_{mm}	the mutual impedance between axial slots
Z_n^b	the mutual impedance between the two axial slots
w_1, w_2	weigh functions of the error function
p	number of columns
h_k	asymmetrical modified Taylor pattern
R	right
L	left
SLL_R	right side lobe level
SLL_L	left side lobe level
ω	angular frequency
μ	magnetic permeability
β	phase constant
ρ	the radius of the waveguide
h	Cut off wave number
α_n	n^{th} slot's central angle
B_{mn}	backward-scattered equation
mn	propagation mode
Subscript t	the tangential field in the cross-section
Subscript S	indicates the cross-section of the uniform waveguide
$\bar{E}_s$	electrical field distributed across the slot
C_{mn}	forward-scattered equatio
β_{11}	the propagation constant of the TE_{11} mode
J	Bessel function
J_1'	derivative of first-order Bessel function
h_ρ	component of the wave vector in cylindrical waveguide along the radius
Z_0	the free impedance of the environment
I_n	current flowing through the n^{th} slot
Y_n^{2w}	slot's self-admittance
Y_n^{2wL}	load's admittance
u_{in}	coefficients of the normalized self-impedance
p_i	the real part of normalized self-impedance
S_i	the imaginary part of the normalized self-impedance
L_i	length of slots

Z_n^{self}	nth slot's self-impedance
Y_{12}	mutual admittance between slot 1 and 2
E_2	Electrical far-field due to the excitation voltage V_2 at slot 2
H_1^*	conjugate radiated magnetic far-field in the response of voltage V_1 of slot 1

APPENDIX A

A. FIRST AND SECOND DESIGN EQUATION DERIVATION

1) CALCULATION OF THE SCATTERING EQUATIONS OF THE AXIAL SLOT ON THE CYLINDRICAL WAVEGUIDE

The formulation of the design equations used in this paper is similar to that proposed by Elliot [16] for a broad wall slot antenna design.

For the dominant mode TE_{11} the field components are expressed as:

$$H_z = J_1(h\rho)\cos(\varphi)\, e^{\pm j\beta_{11}z} \tag{A.1}$$

$$H_\rho = \mp\frac{j\beta}{h}J_1'(h\rho)\cos(\varphi)\, e^{\mp j\beta_{11}z} \tag{A.2}$$

$$H_\varphi = \pm\frac{j\beta}{h^2\rho}J_1(h\rho)\sin(\varphi)\, e^{\mp j\beta_{11}z} \tag{A.3}$$

$$E_\rho = \frac{\omega\mu}{\beta}H_\varphi, \quad E_\varphi = -\frac{\omega\mu}{\beta}H_\rho, \; E_z = 0 \tag{A.4}$$

where ω, μ, β, ρ, h are angular frequency, magnetic permeability, phase constant, the radius of the waveguide, and cutoff number defined as $\frac{1.841}{a}$ which "a" is the radius of the cylinder respectively.

The electric field along the φ direction is:

$$E_\varphi = \frac{V_n^s}{\alpha a}\cos\left(\frac{\pi z}{L_n}\right)\begin{cases} -\dfrac{L_n}{2} < z < \dfrac{L_n}{2} \\ -\dfrac{\alpha}{2} < \varphi < \dfrac{\alpha}{2} \end{cases} \quad \alpha \to 0 \tag{A.5}$$

$$\mathrm{E_s} = \mathrm{E}_\varphi\bar{\mathrm{u}}_\varphi, \quad E_z = 0 \tag{A.6}$$

where L_n is the length of the n'th slot and V_n^s is the maximum voltage distributed across the n'th slot, α is the radius of the cylinder, α_n is the n'th slot's central angle (angle difference between the tip and the end of a typical slot concerning the center of the axis of the cylinder), " $\alpha_n \times a$" is the width of the n'th slot which equals to the length of the arc of a slot on wall of the cylinder.

So the transverse magnetic field at the backward scattering plane, transverse magnetic field at the scattering plane, and also transverse electric field at the scattering plane are:

$$\overline{\mathrm{H}}_{\mathrm{tB}} = \mathrm{H}_\rho\bar{\mathrm{a}}_\rho + \mathrm{H}_\varphi\bar{\mathrm{a}}_\varphi - \mathrm{H}_z\bar{\mathrm{a}}_z \tag{A.7}$$

$$\overline{\mathrm{H}}_{\mathrm{tC}} = \mathrm{H}_\rho\bar{\mathrm{a}}_\rho + \mathrm{H}_\varphi\bar{\mathrm{a}}_\varphi + \mathrm{H}_z\bar{\mathrm{a}}_z \tag{A.8}$$

$$\overline{\mathrm{H}}_{\mathrm{at}} = \mathrm{H}_\rho\bar{\mathrm{u}}_\rho + \mathrm{H}_\varphi\bar{\mathrm{u}}_\varphi \tag{A.9}$$

respectively, where the subscript α is shorthand for the double index "mn".

Following Elliot's [16, pp89-99], we have:

$$B_{mn} = \frac{\int_{slot}\overline{E_s}\times\bar{H}_{tC}\cdot\overline{ds}}{2\int_S \bar{E}_{at}\times\bar{H}_{at}\bar{u}_z ds} \tag{A.10}$$

where B_{mn} is the backward-scattered equation, while its subscript mn corresponds to the propagation mode. The subscript t indicates the tangential field in the cross-section, and the subscript S indicates the cross-section of the uniform waveguide, and the term "Slot" is the slot surface area, and the $\overline{E_s}$ is the electrical field distributed across the slot.

$$B_{11} = -C_{11} = -\frac{V^s J_1(ha)\,h^2}{\omega\mu\beta_{11}} \times \frac{L\cos\left(\frac{\beta_{11}L}{2}\right)\cos(\varphi_0)}{\left(\pi^2-(\beta_{11}L)^2\right)\int_0^a\left(\frac{J_1^2(h\rho)}{h^2\rho}+\rho J_1'^2(h\rho)\right)d\rho} \tag{A.11}$$

Similarly, for the forward-scattered equation for an axial slot on the cylindrical waveguide C_{mn}:

$$C_{mn} = \frac{\int_{slot}\overline{E_s}\times\bar{H}_{tB}\cdot\overline{ds}}{2\int_S \bar{E}_{at}\times\bar{H}_{at}\bar{u}_z ds} \tag{A.12}$$

$$C_{mn} = \frac{VJ_1(ha)h^2}{\omega\mu\beta}\frac{L\cos\left(\frac{\beta L}{2l}\right)\cos(\varphi_0)}{\left(\pi^2-(\beta L)^2\right)\int_0^a\left(\frac{J_1^2(h\rho)}{h^2\rho}+\rho J_1'^2(h\rho)\right)d\rho} \tag{A.13}$$

So for TE_{11}:

$$B_{11} = -C_{11} = -\frac{V^s J_1(ha)\,h^2}{\omega\mu\beta_{11}} \times \frac{L\cos\left(\frac{\beta_{11}L}{2}\right)\cos(\varphi_0)}{\left(\pi^2-(\beta_{11}L)^2\right)\int_0^a\left(\frac{J_1^2(h\rho)}{h^2\rho}+\rho J_1'^2(h\rho)\right)d\rho} \tag{A.14}$$

where B_{11} is the propagation constant of TE_{11}, J is Bessel function, $J_1'^1$ is derivative of first-order Bessel function, and $h\rho$ is a wave vector component in cylindrical waveguide along the radius.

The relation (A.14) can be presented as Fig. 9.

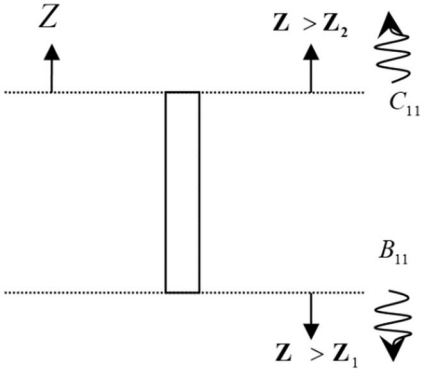

FIGURE 9. The direction of scattering parameters due to the slot's position.

As seen from C_{11}, equation (A.14), forward and backward traveling wave Equations are equal but different in phase; consequently, the transmission line equivalent circuit consists of only series impedance, as shown in Fig. 10.

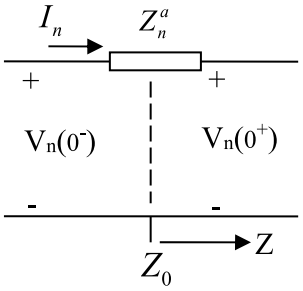

FIGURE 10. The transmission line of the n[th] element.

B. EXTRACTING THE FIRST DESIGN EQUATION FOR AN AXIAL SLOT ON A CYLINDRICAL WAVEGUIDE SLOT IN THE TE11 MODE

To acquire the first equation, it is necessary to write the power equation for the slot. The reflection power from a slot for the TE_{11} is:

$$\begin{aligned} P_{ref} &= \frac{1}{2}\,\mathrm{Re}\int_S \left(\bar{E}_t \times \bar{H}_t^*\right)\cdot \overline{ds} \\ &= \frac{1}{2}\,\mathrm{Re}\int_{S1} \left(B_{11}\bar{E}_{11,t} \times B_{11}^*\bar{H}_{11,t}^*\right).\overline{a_z}ds \\ &= \frac{1}{2}\,\mathrm{Re}\left[\int_{S1}\frac{\omega\mu}{\beta_{11}}\left(\left|H_\varphi\right|^2+\left|H_\rho\right|^2\right)\overline{a_z}\cdot\overline{a_z}ds\right]B_{11}B_{11}^* \\ &= \frac{\omega\mu\beta_{11}\pi}{2h^2}\left[\int_0^a\left(\frac{J_1^2(h\rho)}{h^2\rho}+\rho J_1'^2(h\rho)\right)d\rho\right]B_{11}B_{11}^* \end{aligned} \tag{A.15}$$

where

$$E_t = \begin{cases} B_{11}E_{at} & z < z_1 \\ C_{11}E_{at} & z > z_2 \end{cases} \tag{A.16}$$

The equation of the equivalent transmission line is:

$$\begin{cases} V(z) = (A+C)\,e^{-j\beta z} \\ I(z) = G_0\,(A+C)\,e^{-j\beta z} \end{cases} \quad z > 0 \tag{A.17}$$

From Fig. 9 and using equation (A.17), we have:

$$B = -C = \frac{1}{2}Z^a I_n \tag{A.18}$$

The equivalent power in the transmission line model is equal to:

$$P_{ref,TL} = \frac{1}{2}V^-(z)\,I^{-*}(z) = -\frac{1}{2}\frac{BB^*}{Z_0} \tag{A.19}$$

using (A.15) and (A.19):

$$j\frac{1}{\sqrt{2}}\frac{|B|}{\sqrt{Z_0}} = \sqrt{\frac{\omega\mu\beta\pi}{2h^2}\left[\int_0^a\left(\frac{J_1^2(h\rho)}{h^2\rho}+\rho J_1'^2(h\rho)\right)d\rho\right]} * |B_{11}| \tag{A.20}$$

Substituting the amplitude of equation (A.18) i.e., $|B|$ and equation (A.14) i.e., $|B_{11}|$ we get:

$$j\frac{1}{\sqrt{2}}\frac{\frac{1}{2}I_nZ_n^a}{\sqrt{Z_0}} = \sqrt{\frac{\omega\mu\beta\pi}{2h^2}\left[\int_0^a\left(\frac{J_1^2(h\rho)}{h^2\rho}+\rho J_1'^2(h\rho)\right)d\rho\right]} \times \frac{V_n^s J_1(ha)\,h^2}{\omega\mu\beta} \times N \tag{A.21}$$

Which

$$N = \frac{Lcos\left(\frac{\beta L}{2l}\right)cos(\varphi_0)}{\left(\pi^2-(\beta L)^2\right)\int_0^a\left(\frac{J_1^2(h\rho)}{h^2\rho}+\rho J_1'^2(h\rho)\right)d\rho}$$

Sorting Equation in terms of $\frac{Z_n^a}{Z_0}$:

$$\frac{Z_n^a}{Z_0} = -j\sqrt{\frac{4\pi h^2 J_1^2(ha)}{\omega\mu\beta Z_0\left[\int_0^a\left(\frac{J_1^2(h\rho)}{h^2\rho}+\rho J_1'^2(h\rho)\right)d\rho\right]}} \times \frac{Lcos\left(\frac{\beta L}{2l}\right)cos(\varphi_0)}{\left(\pi^2-(\beta L)^2\right)}\frac{V_n^s}{I_n} \tag{A.22}$$

The first design equation is derived:

$$\frac{Z_n^a}{Z_0} = Kf_n\frac{V_n^s}{I_n} \tag{A.23}$$

where:

$$f_n = \frac{L_n\cos\left(\frac{\beta_{11}L_n}{2}\right)\cos(\varphi_{0n})}{\left(\pi^2-(\beta_{11}L_n)^2\right)} \tag{A.24}$$

and

$$K = -j\sqrt{\frac{4\pi h^2 J_1^2(ha)}{\omega\mu\beta_{11}Z_0\left[\int_0^a\left(\frac{J_1^2(h\rho)}{h^2\rho}+\rho J_1'^2(h\rho)\right)d\rho\right]}} \tag{A.25}$$

where Z_n^a is the active impedance of the n'th slot, Z_0 is the free impedance of the environment, I_n is the current flowing through the n'th slot, and f_n is a factor that includes the slot array's parameters.

C. EXTRACTING THE SECOND DESIGN EQUATION OF THE CYLINDRICAL WAVEGUIDE SLOT FOR THE TE11 MODE

The design steps for the second design equation are similar to that of the first. Using Babinet's principle [16], the dual waveguide axial slot array can be considered an equivalent model of an array of the dipole antenna, arranged in a perfect, infinite conductive ground plane. Besides, another critical assumption is made. It is assumed that any slot is fed in the center via the dual-wire network. If the distribution of the voltage and current for the slot and equivalent dipole are equal, then the half-plane radiation of the slot and its equivalent dipole will be the same. An impedance/admittance circuit with a dual-wire power feeding system must be added to the slot and its dual to equalize their impedance characteristics.

The additional load can model higher-order scattering modes. In this case, the slot's equivalent circuit of the dual-wire feeding system is as follows:

$$I_n^{2w} = \sum_{m=1}^{N} V_m^s Y_{nm}^{2w} \tag{A.26}$$

$$Y_{nn}^{2w} = Y_n^{2w} + Y_n^{2wL} \tag{A.27}$$

where Y_n^{2w} is a slot's self-admittance, and Y_n^{2wL} is the load's admittance which considered for the slot,

The above expressions hold for the equivalent dipole, as well, so:

$$V_n^d = \sum_{m=1}^{N} I_m^d Z_{nm}^d \tag{A.28}$$

$$Z_{nn}^d = Z_n^d + Z_n^{d,L} \tag{A.29}$$

Z_{nn} is the axial slot self-impedance and Z_{nm} is the mutual impedance between axial slots on the guided cylinder, which equals $\sum_{\substack{m=1 \\ m\neq n}}^{N} \frac{V_m^s}{V_n^s} Z_{nm}^d$.

$$Y_n^{2w} = \left(\frac{2}{\eta^2}\right) Z_n^d, \quad Y_{nm}^{2w} = \left(\frac{2}{\eta^2}\right) Z_{nm}^d \tag{A.30}$$

By substituting (A.33) into (A.34), we have:

$$Z_n^{da} = \frac{V_n^d}{I_n^d} = \sum_{m=1}^{N} \frac{I_m^d}{I_n^d} Z_{nm}^d = Z_n^d + Z_n^{dL} + \sum_{\substack{m=1 \\ n\neq m}}^{N} \frac{I_m^d}{I_n^d} Z_{nm}^d \tag{A.31}$$

On the other hand:

$$Y_n^{2wa} = \frac{I_n^{2w}}{V_n^s} = \sum_{m=1}^{N} \frac{V_m^s}{V_n^s} Y_{nm}^{2w} = Y_n^{2w} + Y_n^{2wL} + \sum_{\substack{m=1 \\ n\neq m}}^{N} \frac{V_m^s}{V_n^s} Y_{nm}^{2w} \tag{A.32}$$

$$Y_n^{2wL} = \left(\frac{2}{\eta^2}\right) Z_n^{dL} \tag{A.33}$$

$$\frac{1}{2} I_n I_n^* Z_n^{a*} = \left(\frac{1}{2} V_n^s I_n^{2w*}\right)^* = \frac{1}{2} V_n^d I_n^{d*} \tag{A.34}$$

$$\begin{aligned} \left(V_n^s I_n^{2w*}\right)^* &= V_n^{s*} I_n^{2w} = V_n^{s*} \sum_{m=1}^{N} V_m^s Y_{nm}^{2w} \\ &= V_n^{s*} V_n^s \sum_{m=1}^{N} \frac{V_m^s}{V_n^s} \left(\frac{2}{\eta^2}\right) Z_{nm}^d \\ &= \left(\frac{2}{\eta^2}\right) Z_n^{d,\,a} V_n^{s*} V_n^s \end{aligned} \tag{A.35}$$

From equations (A.34) and (A.35), we have:

$$I_n I_n^* Z_n^{a*} Z_n^a = \left(\frac{2}{\eta^2}\right) Z_n^{da} V_n^{s*} V_n^s Z_n^a \tag{A.36}$$

In the above equation, I_n, V_n^s and Z_n^a are the mode current, the slot voltage, and the active impedance of the n'th slot, respectively, and Z_n^{da} is the active loaded dipole impedance equals $Z_n^{d,a} = Z_{nn} + Z_n^b$.

Considering Booker's equation $Z_{nm}^d = \left(\frac{\eta^2}{2}\right) Y_{nm}^s$ and also using equations (A.11), (A.20), and (A.36) the second design equation is derived:

$$\frac{Z_n^a}{Z_0} = \frac{\eta^2}{2} Z_0 |K|^2 \frac{f_n^2}{Z_n^{d,a}} \tag{A.37}$$

where K and f_n are equal to (A.24) and (A.25), respectively.

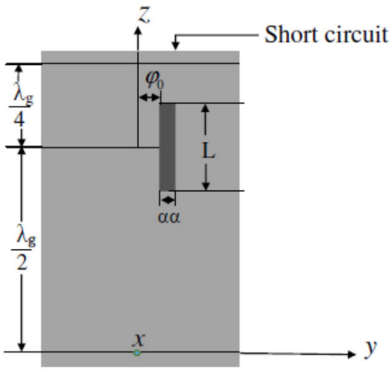

FIGURE 11. The structure of a single axial slot on the circular cylindrical waveguide.

APPENDIX B

A. COMPUTATION OF THE SELF IMPEDANCE AND MUTUAL ADMITTANCE BETWEEN THE TWO AXIAL SLOTS ON THE CYLINDRICAL WAVEGUIDE

Consider an axial slot on a circular cylindrical waveguide shorted at the end, as shown in Fig.11 The radius value is proportional to the different cutoff frequencies. To obtain the desired value for inner and outer radius, we need to calculate them by considering cutoff frequencies. For the proposed slot antenna, the same design considerations have to be done. The inner and outer radii of the conducting cylinder are 11.26mm and 14.06 mm, respectively. The value of the outer radius of the cylinder is obtained by adding T equals 2.8 mm (which could also be enough for the mechanical strength of the aluminum cylinder) to the internal radius value of the cylinder.

The self-admittance of the rectangular slot (having a width of 3.5 mm) is obtained by using HFSS software for an angular step of. 3 degrees. Table 3 & 4 show the results, while Figure 12 depicted real and imaginary parts of normalized self-admittance.

Where $\boldsymbol{u}_{in}$ is the coefficients of the normalized self-impedance, p_i is the real part of normalized self-impedance, and S_i is the imaginary part of the normalized self-impedance.

TABLE 3. Coefficients of the real component of normalized self-impedance.

Real	u_{i5}	u_{i4}	u_{i3}	u_{i2}	u_{i1}	u_{i0}
P_{10}	-0.0000023	0.000575	0.04809	1.3568	-6.7782	430.46
P_9	0.0000370	-0.009340	0.78645	-22.3690	111.9500	-6991.89
P_8	-0.0002600	0.067690	-5.73280	164.4120	-822.7930	50562.55
P_7	0.0011240	-0.287570	24.52550	-709.2580	3542.3300	-214296.00
P_6	-0.0030800	0.793646	-68.17560	1988.2200	-9890.5100	589278.30
P_5	0.0057330	-1.486510	128.64470	-3783.5000	18709.1400	-1098257.00
P_4	-0.0073200	1.913414	-166.85400	4948.9200	-24278.4000	140470.00
P_3	0.0063530	-1.671170	146.86800	-4393.0300	21339.9800	-1217440.00
P_2	-0.0035700	0.947827	-83.96090	2532.5100	-12159.3000	684281.30
P_1	0.0011700	-0.315230	28.15013	-856.1630	4056.1160	-25267.00
P_0	-0.0001000	0.046690	-4.20360	128.9090	601.6560	32991.90

TABLE 4. Coefficients of the imaginary components of normalized self-impedance.

Im	v_{i5}	v_{i4}	v_{i3}	v_{i2}	v_{i1}	v_{i0}
S_8	-0.00000042	0.0000788	-0.004820	0.155010	-4.04537	-36.2294
S_7	0.00000552	-0.0010000	0.061750	-1.933280	51.03370	399.8420
S_6	-0.00003100	0.0057190	-0.343090	10.454200	-278.98000	-1837.9700
S_5	0.00009830	-0.0181400	1.079680	-32.019300	863.02100	4510.0090
S_4	-0.00019000	0.0355950	2.104227	60.763270	-1652.13000	-6223.2500
S_3	0.00023900	-0.0442100	2.599692	-73.167800	2003.87000	4485.5860
S_2	-0.00018000	0.0339400	-1.987350	54.593400	-1503.55000	-1012.9400
S_1	0.00007950	-0.0147100	0.859030	-23.073100	637.94800	-570.7360
S_0	-0.00001500	0.0027570	-0.160670	4.227637	-117.16600	285.5416

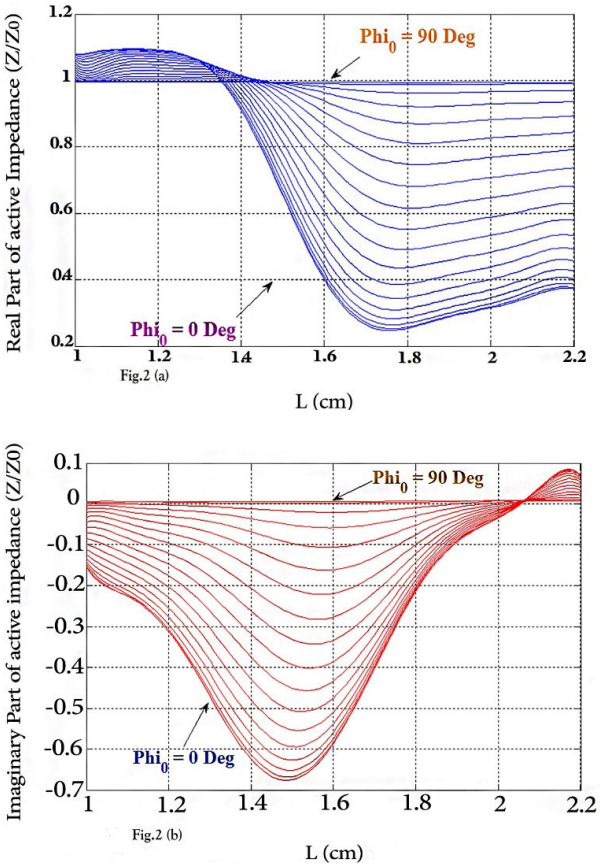

FIGURE 12. The graph of normalized real (a) and imaginary part impedance (b).

The acquired data from Fig.14 can be curve-fitted into two polynomials of orders 8 and 10 as follows:

$$\text{Imaginary}\left(\frac{Z}{Z_0}\right) = \sum_{i=0}^{8} s_i * L^i \tag{B.1}$$

where $s_i = \sum_{k=0}^{5} v_{ik} * \theta^k$

$$\text{Real}\left(\frac{Z}{Z_0}\right) = \sum_{i=0}^{10} p_i * L^i \tag{B.2}$$

where $p_i = \sum_{k=0}^{5} u_{ik} * \theta^k$.

Terms S_i, P_i, and L^i are coefficients of the imaginary components of the normalized self-impedance, coefficients of the imaginary components of the normalized self-impedance, and length of slots, respectively.

Then for the n'th slot self-admittance, we have:

$$\frac{Z_n^{self}}{Z_0} = \text{Real}\left(\frac{Z_n^{self}}{Z_0}\right) + j\,\text{Imaginary}\left(\frac{Z_n^{self}}{Z_0}\right) \tag{B.3}$$

where Z_n^{self} is the n'th slot's self-impedance and Z_0 is the characteristic impedance of the cylindrical waveguide

B. COMPUTATION OF MUTUAL ADMITTANCE BETWEEN THE TWO AXIAL SLOTS ON THE CYLINDRICAL WAVEGUIDE

The computation of the mutual admittance between two axial slots on a cylinder by the extended Poynting's vector was described in [27]. This method is applied here to obtain the mutual admittance between two axial apertures, called 1 and 2.

The integral variables are at spherical coordinates so, the general relationship used here is:

$$Y_{12} = \frac{1}{V_2 V_1^*} \int_c \int_0^{2\pi} E_2 \times H_1^* . \hat{n} r^2 \sin\theta d\theta d\varphi \tag{B.4}$$

where Y_{12} is the mutual admittance between slot 1 and 2, E_2 is the Electrical far-field due to the excitation voltage V_2 at slot 2, and H_1^* is the conjugate radiated magnetic far-field in the response of voltage V_1 of slot 1.

Following far-field relations we have:

$$\mathbf{E}_2 = \mathrm{E}_{2\theta}\hat{\mathrm{a}}_\theta + \mathrm{E}_{2\varphi}\hat{\mathrm{a}}_\varphi \tag{B.5}$$

$$\mathbf{H}_1 = \mathrm{H}_{1\theta}\hat{\mathrm{a}}_\theta + \mathrm{H}_{1\varphi}\hat{\mathrm{a}}_\varphi \tag{B.6}$$

$$\mathrm{H}_\varphi = \frac{\mathrm{E}_\theta}{\eta}, \quad \mathrm{H}_\theta = -\frac{\mathrm{E}_\varphi}{\eta} \tag{B.7}$$

$$\begin{aligned} \boldsymbol{E}_2 \times \boldsymbol{H}_1^* &= \left(E_{2\theta}\hat{a}_\theta + E_{2\varphi}\hat{a}_\varphi\right) \times \left(H_{1\theta}\hat{a}_\theta + H_{1\varphi}\hat{a}_\varphi\right) \\ &= \left(E_{2\theta}{H_{1\varphi}}^* - E_{2\varphi}{H_{1\theta}}^*\right)\hat{a}_r \\ &= \left(E_{2\theta}\frac{{E_{1\theta}}^*}{\eta} + E_{2\varphi}\frac{{E_{1\varphi}}^*}{\eta}\right)\hat{a}_r \end{aligned} \tag{B.8}$$

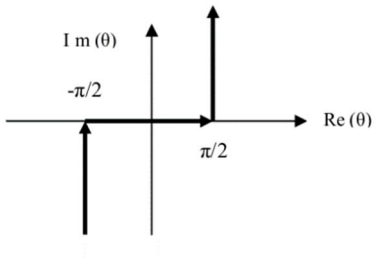

FIGURE 13. The path of integrating.

Considering the Fig.13, the path of integrating c is as follows:

We assume that, in cylindrical coordinates, the positions of slots 1 and 2 are: $(a \cdot \varphi_2 \cdot z_2)$, $(a \cdot \varphi_1 \cdot z_1)$ so the electric and magnetic far-fields regarding the above coordinates will be:

$$\mathrm{E}_{1\varphi} = -\frac{\mathrm{V}_1 \mathrm{e}^{-\mathrm{jkr}_1}}{\pi \mathrm{ar}_1 \mathrm{L}_1} \frac{\cos\left(\frac{\mathrm{kL}_1}{2}\cos(\theta)\right)}{\left[\mathrm{k}^2\cos^2(\theta) - \left(\frac{\pi}{\mathrm{L}_1}\right)^2\right]} \times \sum_{\mathrm{n}=-\infty}^{\infty} \frac{\mathrm{j}^{\mathrm{n}} \mathrm{e}^{\mathrm{jn}(\varphi-\varphi_1)}}{\mathrm{H}_{\mathrm{n}}^{(2)\prime}(\mathrm{kasin}(\theta))} \mathrm{sinc}\left(\frac{\mathrm{n}\varphi_0}{\pi}\right)$$

Here r_1 is equal to

$$r_1 \approx r - z_1 k \cos(\theta) \tag{B.9}$$

and $E_\theta = 0$

For $\mathrm{E}_{2\varphi}$

$$\mathrm{E}_{2\varphi} = -\frac{\mathrm{V}_2 \mathrm{e}^{-\mathrm{jkr}_2}}{\pi \mathrm{ar}_2 \mathrm{L}_2} \frac{\cos\left(\frac{\mathrm{kL}_2}{2}\cos(\theta)\right)}{\left[\mathrm{k}^2\cos^2(\theta) - \left(\frac{\pi}{\mathrm{L}_2}\right)^2\right]} \times \sum_{\mathrm{m}=-\infty}^{\infty} \frac{\mathrm{j}^{\mathrm{m}} \mathrm{e}^{\mathrm{jm}(\varphi-\varphi_2)}}{\mathrm{H}_{\mathrm{n}}^{(2)\prime}(\mathrm{kasin}(\theta))} \mathrm{sinc}\left(\frac{\mathrm{m}\varphi_0}{\pi}\right)$$

Here r_2 is equal to

$$r_2 \approx r - z_2 k \cos(\theta) \tag{B.10}$$

for $E_2 \times H_1^*$ we have:

$$\boldsymbol{E}_2 \times \boldsymbol{H}_1^* = \left(E_{2\varphi} \frac{E_{1\varphi}}{\eta}^*\right) \hat{a}_r$$

To determine the term $E_{2\varphi} \frac{E_{1\varphi}}{\eta}^*$ we need to find $E_{1\varphi}^*$ so:

$$E_{1\varphi}^* = -\frac{V_1^* e^{jk_1}}{\pi a r_1 L_1} \frac{\cos\left(\frac{kL_1}{2}\cos(\theta)\right)}{\left[k^2\cos^2(\theta) - \left(\frac{\pi}{L_1}\right)^2\right]} \times \sum_{n=-\infty}^{\infty} \frac{(-j)^n e^{-jn(\varphi-\varphi_1)}}{\left(H_n^{(2)\prime}(kasin(\theta))\right)^*} sinc\left(\frac{n\varphi_0}{\pi}\right) \tag{B.11}$$

$$E_{2\varphi} = -\frac{V_2 e^{-jkr_2}}{\pi a r_2 L_2} \frac{\cos\left(\frac{kL_2}{2}\cos(\theta)\right)}{\left[k^2\cos^2(\theta) - \left(\frac{\pi}{L_2}\right)^2\right]} \times \sum_{m=-\infty}^{\infty} \frac{j^m e^{jm(\varphi-\varphi_2)}}{H_n^{(2)}(kasin(\theta))} sinc\left(\frac{m\varphi_0}{\pi}\right) \tag{B.12}$$

$$E_{2\varphi} \frac{E_{1\varphi}^*}{\eta} = \frac{V_1^* V_2 e^{-jk(r_2-r_1)}}{\eta\pi^2 r_1 r_2 a^2 L_2 L_1} \frac{\cos\left(\frac{kL_1}{2}\cos(\theta)\right)}{\left[k^2\cos^2(\theta) - \left(\frac{\pi}{L_1}\right)^2\right]} \times \frac{\cos\left(\frac{kL_2}{2}\cos(\theta)\right)}{\left[k^2\cos^2(\theta) - \left(\frac{\pi}{L_2}\right)^2\right]} \cdot \mathrm{A}'$$

$$A' = \sum_{m=-\infty}^{\infty} \sum_{n=-\infty}^{\infty} \frac{j^{m-n} e^{jm(\varphi-\varphi_2)} e^{-jn(\varphi-\varphi_1)}}{H_m^{(2)'}(kasin(\theta)) H_n^{(2)'*}(kasin(\theta))} \times sinc\left(\frac{n\varphi_0}{\pi}\right) sinc\left(\frac{m\varphi_0}{\pi}\right) \tag{B.13}$$

To obtain Y_{12} we have:

$$\begin{aligned} Y_{12} &= \frac{1}{V_2 V_1^*} \int_c \int_0^{2\pi} \boldsymbol{E}_2 \times \boldsymbol{H}_1^* . \hat{n} r^2 \sin\theta d\theta d\varphi \\ &= \frac{1}{V_2 V_1^*} \int_c \int_0^{2\pi} \left(E_{2\varphi} \frac{E_{1\varphi}}{\eta}^*\right) \hat{a}_r . \hat{a}_r r^2 \sin\theta d\theta d\varphi \\ &= \frac{1}{V_2 V_1^*} \int_c \int_0^{2\pi} \frac{V_1^* V_2 e^{-jk(r_2-r_1)}}{\eta\pi^2 r_1 r_2 a^2 L_2 L_1} \frac{\cos\left(\frac{kL_1}{2}\cos(\theta)\right)}{\left[k^2\cos^2(\theta) - \left(\frac{\pi}{L_1}\right)^2\right]} \\ &\quad \times \frac{\cos\left(\frac{kL_2}{2}\cos(\theta)\right)}{\left[k^2\cos^2(\theta) - \left(\frac{\pi}{L_2}\right)^2\right]} \times B' \end{aligned}$$

$$B' = \sum_{m=-\infty}^{\infty} \sum_{n=-\infty}^{\infty} \frac{j^{m-n} e^{jm(\varphi-\varphi_2)} e^{-jn(\varphi-\varphi_1)}}{H_m^{(2)'}(kasin(\theta)) H_n^{(2)'*}(kasin(\theta))} B''$$

$$B'' = sinc\left(\frac{n\varphi_0}{\pi}\right) sinc\left(\frac{m\varphi_0}{\pi}\right) r^2 \sin\theta d\theta d\varphi \tag{B.14}$$

Given the odd symmetry of the integration path and also the odd symmetry of the function relative to θ, we consider the path of integration as Fig.14.

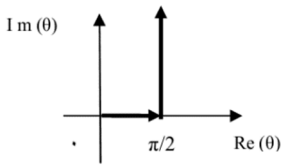

FIGURE 14. Path of integration.

So we have:

$$Y_{12} = \frac{1}{V_2 V_1^*} \int_c \int_0^{2\pi} \left(E_{2\theta} \frac{E_{1\theta}}{\eta}^*\right) r^2 \sin\theta d\theta d\varphi$$

Which C is $= \frac{2}{\eta\pi^2 r_1 r_2 a^2 L_2 L_1} \int_c \int_0^{2\pi} \frac{e^{-jk(r_2-r_1)} cos\left(\frac{kL_1}{2} cos(\theta)\right)}{\left[k^2 cos^2(\theta) - \left(\frac{\pi}{L_1}\right)^2\right]}$

$\frac{cos\left(\frac{kL_2}{2} cos(\theta)\right)}{\left[k^2 cos^2(\theta) - \left(\frac{\pi}{L_2}\right)^2\right]} C'.$

And C′ is

$$sinc\left(\frac{n\varphi_0}{\pi}\right) sinc\left(\frac{m\varphi_0}{\pi}\right) r^2 \sin\theta d\theta d\varphi \tag{B.15}$$

By replacing r_1 and r_2 and considering the even symmetry concerning the variable φ, the integral is simplified as follows:

$$Y_{12} = \frac{2}{\eta\pi^2 a^2 L_2 L_1} \int_c \int_0^{2\pi} D \tag{B.16}$$

D is

$$\frac{e^{-jkcos(\theta)(z_1-z_2)} cos\left(\frac{kL_1}{2} cos(\theta)\right)}{\left[k^2 cos^2(\theta) - \left(\frac{\pi}{L_1}\right)^2\right]} \frac{cos\left(\frac{kL_2}{2} cos(\theta)\right)}{\left[k^2 cos^2(\theta) - \left(\frac{\pi}{L_2}\right)^2\right]} .D'$$

D' is:

$$\sum_{m=0}^{\infty} \sum_{n=0}^{\infty} \frac{\varepsilon_m \varepsilon_n j^{m-n} \cos(m(\varphi-\varphi_2)) \cos(n(\varphi-\varphi_1))}{H_m^{(2)\prime}(kasin(\theta)) H_n^{(2)\prime *}(kasin(\theta))} D''$$

And D'' is $sinc\left(\frac{n\varphi_0}{\pi}\right) sinc\left(\frac{m\varphi_0}{\pi}\right) \sin\theta d\theta d\varphi$ (B.16)

So here:

$$\varepsilon_m = \begin{cases} 1 & m = 0 \\ 2 & m \neq 0 \end{cases}$$

We know $cos(m(\varphi - \varphi_2))cos(n(\varphi - \varphi_1))$ are orthogonal functions, and the outcome is non-zero if m = n. By calculating the integral concerning the variable φ, the simplified expression is:

$$Y_{12} = \frac{4}{\eta\pi a^2 L_2 L_1} \int_c E$$

$$E = \frac{e^{-jkcos(\theta)(z_1-z_2)} cos\left(\frac{kL_1}{2} cos(\theta)\right)}{\left[k^2 cos^2(\theta) - \left(\frac{\pi}{L_1}\right)^2\right]} \times \frac{cos\left(\frac{kL_2}{2} cos(\theta)\right)}{\left[k^2 cos^2(\theta) - \left(\frac{\pi}{L_2}\right)^2\right]} \sin\theta .E'$$

$$E' = \sum_{n=0}^{\infty} \frac{\varepsilon_n cos(n(\varphi_1-\varphi_2))}{\left|H_n^{(2)\prime}(kasin(\theta))\right|^2} sinc^2\left(\frac{n\varphi_0}{\pi}\right) d\theta \tag{B.17}$$

To calculate the integral, we divide it into two real and imaginary parts, and then we will take a step to calculate it.

For the real part:

$$k_z = kcos(\theta) .dk_z = -k \sin\theta d\theta\theta = \left[0 \frac{\pi}{2}\right] \rightarrow k_z = [k0]$$

Let us take the imaginary part of the path. First, we reconstruct the path. That is, we have a new path:

$$k_z = kcos(\theta) = kcos(Re(\theta) + jIm(\theta))$$
$$= k\left[cos(Re(\theta)) cosh(Im(\theta)) - jsin(Re(\theta)) sinh(Im(\theta))\right]$$

Now we consider that, $k_z = -jk_z \cdot k_z = [0 \ \infty]$ so we have:

$$Y_{12} = G_{12} + jB_{12} \tag{B.18}$$

$$G_{12} = \frac{4}{\eta\pi a^2 L_2 L_1} \int_0^k \frac{cos\left(\frac{k_z L_1}{2}\right)}{\left[k_z^2 - \left(\frac{\pi}{L_1}\right)^2\right]} \frac{cos\left(\frac{k_z L_2}{2}\right)}{\left[k_z^2 - \left(\frac{\pi}{L_2}\right)^2\right]} F'$$

$$F' = cos(k_z(z_1-z_2)) \sum_{n=0}^{\infty} \frac{\varepsilon_n cos(n(\varphi_1-\varphi_2))}{\left|H_n^{(2)\prime}\left(a\sqrt{k^2-k_z^2}\right)\right|^2} \times sinc^2\left(\frac{n\varphi_0}{\pi}\right) dk_z \tag{B.19}$$

$$B_{12} = \frac{4}{\eta\pi a^2 L_2 L_1} \int_0^{\infty} \frac{\cosh\left(\frac{k_z' L_1}{2}\right)}{\left[k_z'^2 + \left(\frac{\pi}{L_1}\right)^2\right]} \frac{cosh\left(\frac{k_z' L_2}{2}\right)}{\left[k_z'^2 + \left(\frac{\pi}{L_2}\right)^2\right]} L' \tag{B.20}$$

where L' in (B.20) *is:*

$$L' = e^{-jk_z'(z_1-z_2)} \sum_{n=1}^{\infty} \frac{\varepsilon_n cos(n(\varphi_1-\varphi_2))}{\left|H_n^{(2)\prime}\left(a\sqrt{k^2+k_z'^2}\right)\right|^2} \times sinc^2\left(\frac{n\varphi_0}{\pi}\right) dk_z' - Q' \tag{B.21}$$

Moreover, Q' in (B.21) *is:*

$$Q' = \left[\frac{4}{\eta\pi a^2 L_2 L_1} \int_0^k \frac{cos\left(\frac{k_z L_1}{2}\right)}{\left[k_z^2 - \left(\frac{\pi}{L_1}\right)^2\right]} \frac{cos\left(\frac{k_z L_2}{2}\right)}{\left[k_z^2 - \left(\frac{\pi}{L_2}\right)^2\right]}\right] R' \tag{B.22}$$

Which R' in (B.22) is:

$$R' = sin(k_z(z_1-z_2)) \sum_{n=0}^{\infty} \frac{\varepsilon_n cos(n(\varphi_1-\varphi_2))}{\left|H_n^{(2)\prime}\left(a\sqrt{k^2-k_z^2}\right)\right|^2} \times sinc^2\left(\frac{n\varphi_0}{\pi}\right) dk_z \tag{B.23}$$

REFERENCES

[1] X. S. Fang and K. W. Leung, "Linear-/circular-polarization designs of dual-/wide-band cylindrical dielectric resonator antennas," *IEEE Trans. Antennas Propag.*, vol. 60, no. 6, pp. 2662–2671, Jun. 2012.

[2] H. H. Tran, N. Nguyen-Trong, and A. M. Abbosh, "Simple design procedure of a broadband circularly polarized slot monopole antenna assisted by characteristic mode analysis," *IEEE Access*, vol. 6, pp. 78386–78393, 2018.

[3] M. Abdullah, S. H. Kiani, and A. Iqbal, "Eight element multiple-input multiple-output (MIMO) antenna for 5G mobile applications," *IEEE Access*, vol. 7, pp. 134488–134495, 2019.

[4] R. Xu, J.-Y. Li, and J. Liu, "A design of broadband circularly polarized C-shaped slot antenna with sword-shaped radiator and its array for L/S-band applications," *IEEE Access*, vol. 6, pp. 5891–5896, 2018.

[5] S. Shamsinejad, N. Khalid, F. M. Monavar, S. Shamsadini, R. Mirzavand, G. Moradi, and P. Mousavi, "Pattern reconfigurable cubic slot antenna," *IEEE Access*, vol. 7, pp. 64401–64410, 2019.
[6] Y. J. Li, Z. Y. Lu, and L. S. Yang, "CPW-fed slot antenna for medical wearable applications," *IEEE Access*, vol. 7, pp. 42107–42112, 2019.
[7] R. Xu, J.-Y. Li, J.-J. Yang, K. Wei, and Y.-X. Qi, "A design of U-shaped slot antenna with broadband dual circularly polarized radiation," *IEEE Trans. Antennas Propag.*, vol. 65, no. 6, pp. 3217–3220, Jun. 2017.
[8] Z. Chen, H. Liu, J. Yu, and X. Chen, "High gain, broadband and dual-polarized substrate integrated waveguide cavity-backed slot antenna array for 60 GHz band," *IEEE Access*, vol. 6, pp. 31012–31022, 2018.
[9] W. Yuan, X. Liang, L. Zhang, J. Geng, W. Zhu, and R. Jin, "Rectangular grating waveguide slot array antenna for SATCOM applications," *IEEE Trans. Antennas Propag.*, vol. 67, no. 6, pp. 3869–3880, Jun. 2019.
[10] Y. Jia, Y. Liu, W. Zhang, J. Wang, and G. Liao, "In-band radar cross section reduction of slot array antenna," *IEEE Access*, vol. 6, pp. 23561–23567, Jan. 2018.
[11] M. N. Y. Koli, M. U. Afzal, K. P. Esselle, and R. M. Hashmi, "An all-metal high-gain radial-line slot-array antenna for low-cost satellite communication systems," *IEEE Access*, vol. 8, pp. 139422–139432, 2020.
[12] R. Lian, Z. Wang, Y. Yin, J. Wu, and X. Song, "Design of a low-profile dual-polarized stepped slot antenna array for base station," *IEEE Antennas Wireless Propag. Lett.*, vol. 15, pp. 362–365, 2016.
[13] H. Oraizi and M. T. Noghani, "Design and optimization of waveguide-fed centered inclined slot arrays," *IEEE Trans. Antennas Propag.*, vol. 57, no. 12, pp. 3993–3997, Dec. 2009.
[14] A. F. Stevenson, "Theory of slots in rectangular wave-guides," *J. Appl. Phys.*, vol. 19, no. 1, pp. 24–38, 1948.
[15] A. Oliner, "The impedance properties of narrow radiating slots in the broad face of rectangular waveguide: Part I—Theory," *IRE Trans. Antennas Propag.*, vol. 5, no. 1, pp. 4–11, Jan. 1957.
[16] R. S. Elliott, *Antenna Theory and Design*. Upper Saddle River, NJ, USA: Prentice-Hall, 2003.
[17] H. Oraizi, A. K. Behbahani, M. T. Noghani, and M. Sharafimasouleh, "Optimum design of travelling rectangular waveguide edge slot array with non-uniform spacing," *IET Microw., Antennas Propag.*, vol. 7, no. 7, pp. 575–581, May 2013.
[18] J. R. Wait, *Electromagnetic Radiation From Cylindrical Structures*. New York, NY, USA: Pergamon, 1959.
[19] D. H. Shin and H. J. Eom, "Radiation from narrow axial slots on a conducting circular cylinder," *Radio Sci.*, vol. 41, no. 4, Aug. 2006, Art. no. RS4005.
[20] M. S. Masouleh and A. K. Behbahani, "Optimum design of the array of circumferential slots on a cylindrical waveguide," *AEU, Int. J. Electron. Commun.*, vol. 70, no. 5, pp. 578–583, May 2016.
[21] G. F. Khodae, J. Nourinia, and C. Ghobadi, "A practical miniaturized U-slot patch antenna with enhanced bandwidth," *Prog. Electromagn. Res. B*, vol. 3, pp. 47–62, 2008.
[22] Y. L. Chen, C. L. Ruan, and L. Peng, "A novel ultra-wideband bow-tie slot antenna in wireless communication systems," *Prog. Electromagn. Res. Lett.*, vol. 1, pp. 101–108, 2008.
[23] K. Hashimoto, J. Hirokawa, and M. Ando, "A post-wall waveguide center-feed parallel plate slot array antenna in the millimeter-wave band," *IEEE Trans. Antennas Propag.*, vol. 58, no. 11, pp. 3532–3538, Nov. 2010.
[24] R.-B. Tsai, K.-L. Wong, and H.-C. Su, "Analysis of a microstrip-line-fed radiating slot on a cylindrical surface," *Microw. Opt. Technol. Lett.*, vol. 8, no. 4, pp. 193–196, Mar. 1995.
[25] L. Bailin, "The radiation field produced by a slot in a large circular cylinder," *IRE Trans. Antennas Propag.*, vol. 3, no. 3, pp. 128–137, Jul. 1955.
[26] R. Elliott, "An improved design procedure for small arrays of shunt slots," *IEEE Trans. Antennas Propag.*, vol. AP-31, no. 1, pp. 48–53, Jan. 1983.
[27] E. V. Sohtell, "Mutual admittance between slots on a cylinder using the extended Poynting vector method," *IEE Proc. H, Microw., Antennas Propag.*, vol. 133, no. 3, pp. 238–240, Jun. 1986.
[28] *RF Terminators SMA Male Resistor Cap 50 Ohm*. Accessed: Sep. 17, 2020. [Online]. Available: https://rflambda.com

MAHMOUD SHARAFI MASOULEH received the B.S. degree in electrical engineering and the M.S. degree in electrical engineering specializing in fields and waves from the Iran University of Science and Technology (IUST), Tehran, Iran, in 2008 and 2011, respectively. He is currently pursuing the Ph.D. degree in electrical engineering with the NSF-funded CATE Center, Florida International University (FIU), Miami. He is also a Research Assistant (RA) with the NSF-funded CATE Center, Florida International University (FIU). His M.S. thesis was about novel terahertz microstrip antennas. His research interests include wireless EEG acquiring systems, active amplifier design, design of microwave links, wireless power transfer (WPT) systems, wire-free and battery-less sensors, passive and active RF, and microwave components.

AMIN KARGAR BEHBAHANI received the B.S. degree from the Shahid Chamran University of Ahvaz, Ahwaz, Iran, in 2009, and the M.S. degree from the Iran University of Science and Technology (IUST), Tehran, Iran, in 2012. His current research focuses on slot arrays on the cylindrical and rectangular waveguide. His research interests include microwave/RF passive components and THz antennas.

MALEK ADJOUADI received the B.S. degree in electrical engineering from Oklahoma State University and the M.S. and Ph.D. degrees in electrical engineering from the University of Florida. He has been the Founding Director of the Center for Advanced Technology and Education funded by the National Science Foundation, since 1993. He is currently a Ware Professor with the Department of Electrical and Computer Engineering, Florida International University. His research interests include image and signal processing, assistive technology to help persons with visual disabilities, and brain research, with a focus on Alzheimer's disease and epilepsy.